



Article

On the Role of Cs₄PbBr₆ Phase in the Luminescence Performance of Bright CsPbBr₃ Nanocrystals

Kateřina Děcká ^{1,2,*}, Aděla Suchá ¹, Jan Král ¹, Ivo Jakubec ³, Martin Nikl ², Vítězslav Jarý ², Vladimír Babin ², Eva Mihóková ² and Václav Čuba ¹

¹ Department of Nuclear Chemistry, Faculty of Nuclear Sciences and Physical Engineering, Czech Technical University in Prague, Břehová 7, 115 19 Prague, Czech Republic; suchaade@fffi.cvut.cz (A.S.); kralja13@fffi.cvut.cz (J.K.); vaclav.cuba@fffi.cvut.cz (V.Č.)

² Institute of Physics, Czech Academy of Sciences, Cukrovarnická 10, 162 00 Prague, Czech Republic; nikl@fzu.cz (M.N.); jary@fzu.cz (V.J.); babinv@fzu.cz (V.B.); mihokova@fzu.cz (E.M.)

³ Institute of Inorganic Chemistry, Czech Academy of Sciences, Husinec-Řež č.p. 1001, 250 68 Řež, Czech Republic; jakubec@iic.cas.cz

* Correspondence: Katerina.Decka@fffi.cvut.cz

Abstract: CsPbBr₃ nanocrystals have been identified as a highly promising material for various optoelectronic applications. However, they tend to coexist with Cs₄PbBr₆ phase when the reaction conditions are not controlled carefully. It is therefore imperative to understand how the presence of this phase affects the luminescence performance of CsPbBr₃ nanocrystals. We synthesized a mixed CsPbBr₃-Cs₄PbBr₆ sample, and compared its photo- and radioluminescence properties, including timing characteristics, to the performance of pure CsPbBr₃ nanocrystals. The possibility of energy transfer between the two phases was also explored. We demonstrated that the presence of Cs₄PbBr₆ causes significant drop in radioluminescence intensity of CsPbBr₃ nanocrystals, which can limit possible future applications of Cs₄PbBr₆-CsPbBr₃ mixtures or composites as scintillation detectors.

Keywords: nanocrystals; lead halide perovskites; luminescence; scintillation detectors



Citation: Děcká, K.; Suchá, A.; Král, J.; Jakubec, I.; Nikl, M.; Jarý, V.; Babin, V.; Mihóková, E.; Čuba, V. On the Role of Cs₄PbBr₆ Phase in the Luminescence Performance of Bright CsPbBr₃ Nanocrystals. *Nanomaterials* **2021**, *11*, 1935. <https://doi.org/10.3390/nano11081935>

Academic Editor: Ashish Arora

Received: 2 July 2021

Accepted: 22 July 2021

Published: 27 July 2021

Publisher's Note: MDPI stays neutral with regard to jurisdictional claims in published maps and institutional affiliations.



Copyright: © 2021 by the authors. Licensee MDPI, Basel, Switzerland. This article is an open access article distributed under the terms and conditions of the Creative Commons Attribution (CC BY) license (<https://creativecommons.org/licenses/by/4.0/>).

1. Introduction

Cesium lead halide perovskite quantum dots of the CsPbX₃ (X = Cl, Br, I) formula have been first identified by Nikl et al. group as nano-inclusions in CsX host doped by Pb²⁺ ions [1–3]. However, they have not been studied extensively since the introduction of their colloidal synthesis in 2015 [4]. They were immediately identified as highly promising materials for various applications, mostly for solar cells [5], LEDs [6], or displays [7]. Their excellent luminescent properties, such as high quantum efficiency, narrow emission lines, and fast decay times, are also highly desirable for scintillator manufacture. Recently, a body of studies on the lead halide perovskites has also been focused on their application in X-ray detection [8–14].

Nevertheless, this material also has some drawbacks; in particular its poor chemical stability on air [15,16]. An obvious solution would be provided by encapsulation of CsPbX₃ in various inert matrices such as SiO₂ [17–19], TiO₂ [20], or organic polymers [8,21,22]. Many studies also proposed an interesting composite material CsPbBr₃@Cs₄PbBr₆ which, besides enhanced stability, also passivates CsPbBr₃ nanocrystals, i.e., suppresses non-radiative recombinations on surface defects [23–25]. Various CsPbBr₃-Cs₄PbBr₆ mixtures in the form of two different nanocrystal population were also prepared [26,27].

Cs₄PbBr₆ is a material often referred to as a “zero-dimensional perovskite”, while CsPbBr₃ is called a “three-dimensional perovskite”. CsPbBr₃ consists of corner sharing PbBr₆⁴⁻ octahedra, whereas in Cs₄PbBr₆ those octahedra are isolated (see Figure S1 in Supplementary Information). Cs₄PbBr₆ continues to be somewhat controversial material; there is still an ongoing debate on whether or not it is a source of bright green luminescence

and, if so, what the origin of that luminescence is [28]. There is also a question how the presence of Cs_4PbBr_6 affects the luminescent properties of CsPbBr_3 and vice versa.

The debate was initiated by some early reports on pure Cs_4PbBr_6 crystals with superior green luminescence without any profound considerations about the origin of such luminescence [29,30]. The origin of the green luminescence was questioned, and two major opinions appeared in research community; one strong opinion is that CsPbBr_3 nanoinclusions are, in fact, present in Cs_4PbBr_6 crystals [25,31–33], as the bright green emission is associated with CsPbBr_3 nanocrystals. It has already been stated in 1999 by Nikl et al. that it is difficult to suppress the presence of CsPbBr_3 in Cs_4PbBr_6 completely [34]. This point of view is further supported by many studies on non-luminescent Cs_4PbBr_6 that can be easily transformed into bright CsPbBr_3 [35–39].

The other strong opinion proposes that the green luminescence is due to point defects in Cs_4PbBr_6 structure. Some possible defects that may cause green luminescence were identified, for example the Br vacancy [40–42]. For more details, please refer to review papers published on this subject, for example the most recent, [28], which supports the opinion based on the presence of nanoinclusions, and provides persuasive arguments rebutting the Br vacancy concept.

Understanding of the role of CsPbBr_3 and Cs_4PbBr_6 phases in the luminescence of cesium lead bromides is particularly important when considering applications and future needs to scale-up the production for manufacturing. CsPbBr_3 nanocrystals have been recently identified as highly prospective scintillators for applications requiring fast response, for example a new generation of time-of-flight positron emission tomographs (TOF-PET), or new detectors for high energy physics [43,44]. However, these considerations are important regardless the target application. It is clear that CsPbBr_3 and Cs_4PbBr_6 phases tend to coexist. Therefore, it is evident that this tendency may become a serious issue in a scale-up of the synthesis for industrial production. In order to manufacture a material of the best performance, it is imperative to know how detrimental a contamination of CsPbBr_3 nanocrystals by Cs_4PbBr_6 phase can be, if at all. There have already been some arguments raised in the recent literature against the possible applicability of $\text{CsPbBr}_3@ \text{Cs}_4\text{PbBr}_6$ composite as a scintillator [45].

The band gap energy of Cs_4PbBr_6 and CsPbBr_3 was calculated to be 3.9 eV and 2.3 eV, respectively [46]. This allows an energy transfer from Cs_4PbBr_6 to CsPbBr_3 . This transfer can be both radiative and/or non-radiative. Excitation in Cs_4PbBr_6 phase results in formation of self-trapped excitons that radiatively recombine while emitting UV photons. This emission can radiatively excite CsPbBr_3 . The band alignment in the core-shell structure $\text{CsPbBr}_3@ \text{Cs}_4\text{PbBr}_6$ is of the type I, which means that the valence band maximum and the conduction band minimum are fully within the Cs_4PbBr_6 band gap. This also allows a non-radiative energy transfer from Cs_4PbBr_6 to CsPbBr_3 by hopping [46].

However, when the energy transfer does not occur, the presence of Cs_4PbBr_6 may hinder the luminescence from CsPbBr_3 . In a theoretical model of 80 nm slab of CsPbBr_3 below 10 μm of $\text{CsPbBr}_3@ \text{Cs}_4\text{PbBr}_6$ composite, the escaping emission spectrum was calculated to be 100 \times attenuated compared to the launched spectrum from the CsPbBr_3 slab [38]. The attenuation coefficient of Cs_4PbBr_6 is higher than that of CsPbBr_3 [47], therefore the incident energy will be preferably deposited in the Cs_4PbBr_6 phase.

This study intends to contribute to an intense and important debate about the CsPbBr_3 vs. Cs_4PbBr_6 issue, and also to shed some light on the (radio)luminescence properties of CsPbBr_3 and Cs_4PbBr_6 mixtures, which should help to better understand the dynamics of the abovementioned $\text{CsPbBr}_3@ \text{Cs}_4\text{PbBr}_6$ composite and its applicability in the field of scintillation detectors. In particular, analysis of radioluminescence decays of our materials might provide a valuable set of data on the light and/or energy transfer between the two phases. We reiterate that, unlike rather extended literature on PL properties of materials in question, data on scintillation properties, especially scintillation decays, are scarce.

We synthesized CsPbBr_3 nanocrystals using the hot injection method (HI) [4] and their mixture with Cs_4PbBr_6 crystals using the room-temperature precipitation method

(RTP) [48]. The RTP method is, by its nature (simple mixing of two solutions without any heating), the best candidate for potential scaling up. The HI is the most widely used method, which proves its robustness and reproducibility. We found out that the HI method usually leads to high quality pure CsPbBr₃ nanocrystals, while RTP protocol resulted in various CsPbBr₃-Cs₄PbBr₆ mixtures. We studied and compared luminescent properties of all samples in detail (both photoluminescence and radioluminescence, including decay kinetics) with respect to their composition, structure, and morphology. We found out that the presence of Cs₄PbBr₆ phase significantly deteriorates CsPbBr₃ scintillation light output, which can limit the application potential of CsPbBr₃-Cs₄PbBr₆ mixtures as scintillation detectors.

2. Materials and Methods

2.1. Chemicals

This study utilizes the following chemicals: CsBr (99.999%, Merck, Darmstadt, Germany), PbBr₂ (99.999%, Merck, Darmstadt, Germany), Cs₂CO₃ (99.9%, Merck, Darmstadt, Germany), oleylamine (OAm, 70%, Merck, Darmstadt, Germany), oleic acid (OA, 90%, Merck, Darmstadt, Germany), 1-octadecene (90%, Merck, Darmstadt, Germany), n-hexane (anhydrous, 98%, Merck, Darmstadt, Germany), toluene (99.8%, Merck, Darmstadt, Germany), and *N,N*-dimethylformamide (DMF, anhydrous, 99.8%, Merck, Darmstadt, Germany). All chemicals were used as received, without further purification, unless stated otherwise.

2.2. Hot Injection (HI) Synthesis of Pure CsPbBr₃

The procedure introduced by Protesescu et al. was used [4]. In short, 0.752 mmol of PbBr₂, 20 mL of 1-octadecene (ODE), 2 mL of oleylamine (OAm), and 1.78 mL of oleic acid (OA), were mixed in 100 mL 3-necked flask and degassed at 110 °C under vacuum for 1 h. After that, 0.5 mL of dried pre-synthesized cesium oleate solution (0.4 M) was injected at 170 °C under argon atmosphere. Solid product was separated from ODE solution by centrifugation and redispersed in hexane. For narrowing the size distribution and enhancing colloidal stability, one more centrifugation step was performed, and the supernatant was collected.

The synthesis of cesium oleate was modified according to the study by Lu [49], which provides a complete conversion of cesium salt to cesium oleate, resulting in better reproducibility of synthesis, and in complete solubility of cesium oleate at room temperature by reacting 5 molar equivalents of oleic acid with respect to Cs. The amount of OA added during the CsPbBr₃ synthesis was adjusted to match the molar ratios from [4].

For more details on both syntheses, please refer to Supplementary Information.

2.3. Room-Temperature Precipitation (RTP) Synthesis of CsPbBr₃-Cs₄PbBr₆ Mixture

The procedure introduced by Li et al. [48] as supersaturation recrystallization (currently called room-temperature precipitation) was used with slight modifications for better reproducibility. In short, 0.4 mmol of PbBr₂ and 0.4 mmol of CsBr were dissolved in 10 mL of dimethylformamide (DMF) and 1 mL of OA and 0.5 mL of OAm were added. Then, 1 mL of the solution was quickly added to 10 mL of toluene. Solid product was collected by centrifugation, both the supernatant and the precipitate were characterized. For more details, please refer to Supplementary Information.

2.4. Characterization

X-ray powder diffraction (XRPD) was measured using a Rigaku Miniflex 600 diffractometer equipped with the Cu X-ray tube (average wavelength $\lambda_{\alpha 1,2}$ 0.15418 nm, voltage 40 kV, current 15 mA). Data were collected with a speed of 2° /min and compared with the ICDD PDF-2 database, version 2013. The transmission electron microscopy (TEM) was obtained using an EM201 microscope (Philips, Amsterdam, Netherlands). Absorption spectra were collected using a Cary 100 spectrophotometer (Varian, Palo Alto, CA, USA).

Photoluminescence (PL) excitation and emission spectra were collected using a FluoroMax spectrofluorometer (Horiba Jobin Yvon, Kyoto, Japan). Radioluminescence (RL) spectra were collected using a 5000 M spectrofluorometer (Horiba Jobin Yvon, Kyoto, Japan) with a monochromator and TBX-04 (IBH Scotland, Glasgow, Scotland) photodetector, the excitation source was a Seifert X-ray tube (40 kV, 15 mA). Spectrofluorometer 5000 M (Horiba Jobin Yvon, Kyoto, Japan) was used for measuring PL decay curves using the pulsed nanoLED sources (IBH Scotland, Glasgow, Scotland, excitation wavelengths 310 nm and 389 nm, 80 kHz repetition rate) as the excitation sources. The detection part of the setup involved a single-grating monochromator and a photon counting detector TBX-04 (IBH Scotland, Glasgow, Scotland). RL decay curves were collected using hybrid picosecond photon detector HPPD-860 and Fluorohub unit (Horiba Scientific, Kyoto, Japan). Decays were recorded in both the long and short time windows, as the short time window is relevant for the fast timing applications. Samples were excited by picosecond (ps) X-ray tube N5084 from Hamamatsu, operating at 40 kV. The X-ray tube was driven by the ps light pulser (Hamamatsu, Hamamatsu City, Japan) equipped with a laser diode operating at 405 nm. The instrumental response function FWHM of the setup is about 76 ps. Convolution procedure was applied to all decay curves to determine true decay times (SpectraSolve software package, Ames Photonics, Hurst, TX, USA). The contribution of a component expressed as a percentage (often referred to as a light sum, LS) was calculated as:

$$LS_n = \frac{A_n \tau_n}{\sum A_i \tau_i}$$

where A_n and τ_n denotes amplitude and decay time of the n th component.

XRPD, RL spectra, and RL/PL decays were measured on solid samples, i.e., precipitates after the first centrifugation step. In case of supernatant of sample prepared by RTP, XRPD was measured on drop-casted film. Samples for TEM characterization were obtained by drop-casting the final toluene/hexane solutions on TEM grid. Absorption and PL excitation/emission spectra were also collected on final toluene/hexane solutions.

3. Results and Discussion

XRPD patterns of all samples are presented in Figure 1 and compared to ICDD PDF-2 database records for orthorhombic CsPbBr_3 (#01-072-7929) and rhombohedral Cs_4PbBr_6 (#01-077-8224) phases. The sample prepared by the hot injection (HI) method (red line) was identified as pure CsPbBr_3 sample. The diffraction lines are significantly broadened, suggesting that this phase consists of very small crystallites. Halder–Wagner method of determining linear size of crystallites (using Scherrer constant value 0.94) revealed their mean size as (13 ± 1) nm. A slightly elevated background under 40° , suggesting the presence of an amorphous phase, can be attributed to a small excess of organic ligands (oleic acid and oleylamine) present in the measured sample.

Two diffractograms were recorded for the sample prepared by the room-temperature precipitation method (RTP); precipitated solid sample (green line in Figure 1) and supernatant from centrifugation (blue line). The pattern of the precipitate shows only the presence of Cs_4PbBr_6 phase and elevated background under 40° (i.e., an amorphous phase is present). A higher amount of an amorphous phase suggests a large excess of free organic ligands in this sample. Narrow peaks indicate that this phase has much larger crystallites than those of CsPbBr_3 phase identified in the pure (HI) sample.

To prove the expected presence of CsPbBr_3 nanocrystals in this sample (which was strongly indicated by blue/green luminescence of the sample, see below and also [3,25,31,47]), we also measured a drop-casted film of this sample's supernatant (blue line in Figure 1). Narrow peaks of much lower intensity than in centrifuged sample remain present in this diffractogram. In addition, two broad peaks are present at around 15° and 30° (indicated by red stars). Detailed analysis revealed that the first peak can be attributed to two CsPbBr_3 diffractions from (002) and (110) lattice planes, and the second peak can be attributed to CsPbBr_3 diffractions from (004) and (220) lattice planes. This clearly indicates prefer-

ential orientation of nanocrystalline phase in this direction, suggesting the presence of nanoplatelets. As we have demonstrated, this type of synthesis is indeed capable of producing CsPbBr_3 nanoplatelets in the supernatant [50]. Nevertheless, Figure 1 still provides only a partial evidence of the CsPbBr_3 nanocrystals present in the centrifuged sample, as there are many CsPbBr_3 diffraction lines missing in the pattern.

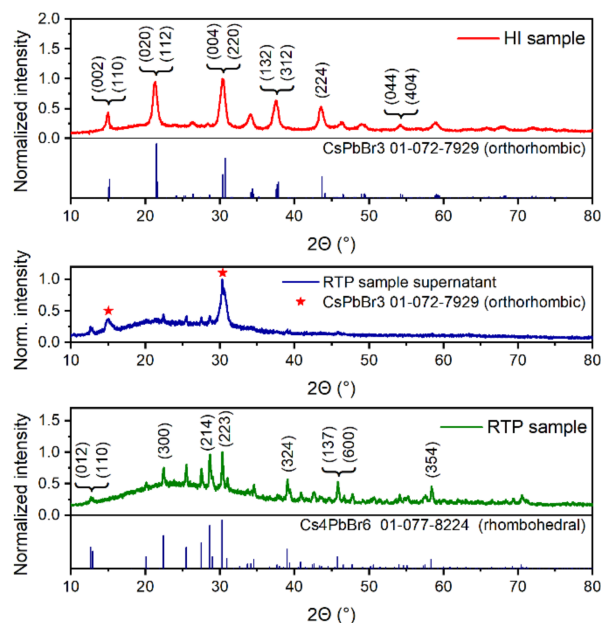


Figure 1. (From top to bottom) XRPD pattern of a precipitate of the sample prepared by the hot injection method (HI, red line) compared to the ICDD PDF-2 database record for CsPbBr_3 ; XRPD pattern of a supernatant of the sample prepared by the room-temperature precipitation method (RTP, blue line), red stars denote positions of the most intense CsPbBr_3 diffraction double lines; and XRPD pattern of a precipitate of the sample prepared by the RTP method (green line) compared to the ICDD PDF-2 database record for Cs_4PbBr_6 .

To provide a stronger evidence of the CsPbBr_3 presence, we performed TEM and analyzed selected area electron diffraction (SAED) patterns of the corresponding micrographs (see Figure 2). TEM in Figure 2a shows that the sample prepared by the HI method (identified by XRPD in Figure 1 as a pure orthorhombic CsPbBr_3 sample with nano-sized crystallites), indeed consists of nanocrystals of cubic shape with the mean size of (19.1 ± 0.2) nm. This value is in good agreement with the calculated mean crystallite size from XRPD pattern in Figure 1. The small discrepancy may be caused by an inaccuracy of determining the FWHM (full width at half maxima) of CsPbBr_3 orthorhombic double peaks and the fact that diffractions at larger angles are partially hidden in the background. TEM in Figure 2b shows that the sample prepared by the RTP method (identified as rhombohedral Cs_4PbBr_6 by XRPD in Figure 1), is clearly a mixture of larger hexagonal crystals (crystal size around 110 nm), and small nanocrystals of roughly cubic shape with the mean size of (9.8 ± 0.2) nm. SAED analysis in Figure 2e–g shows that, in both cases, the cubic nanocrystals can be attributed to the CsPbBr_3 phase, while the hexagonal phase was confirmed as that of Cs_4PbBr_6 . We conclude that the sample prepared by RTP method is, in fact, a mixed sample containing both the CsPbBr_3 nanocrystals and the larger Cs_4PbBr_6 crystals.

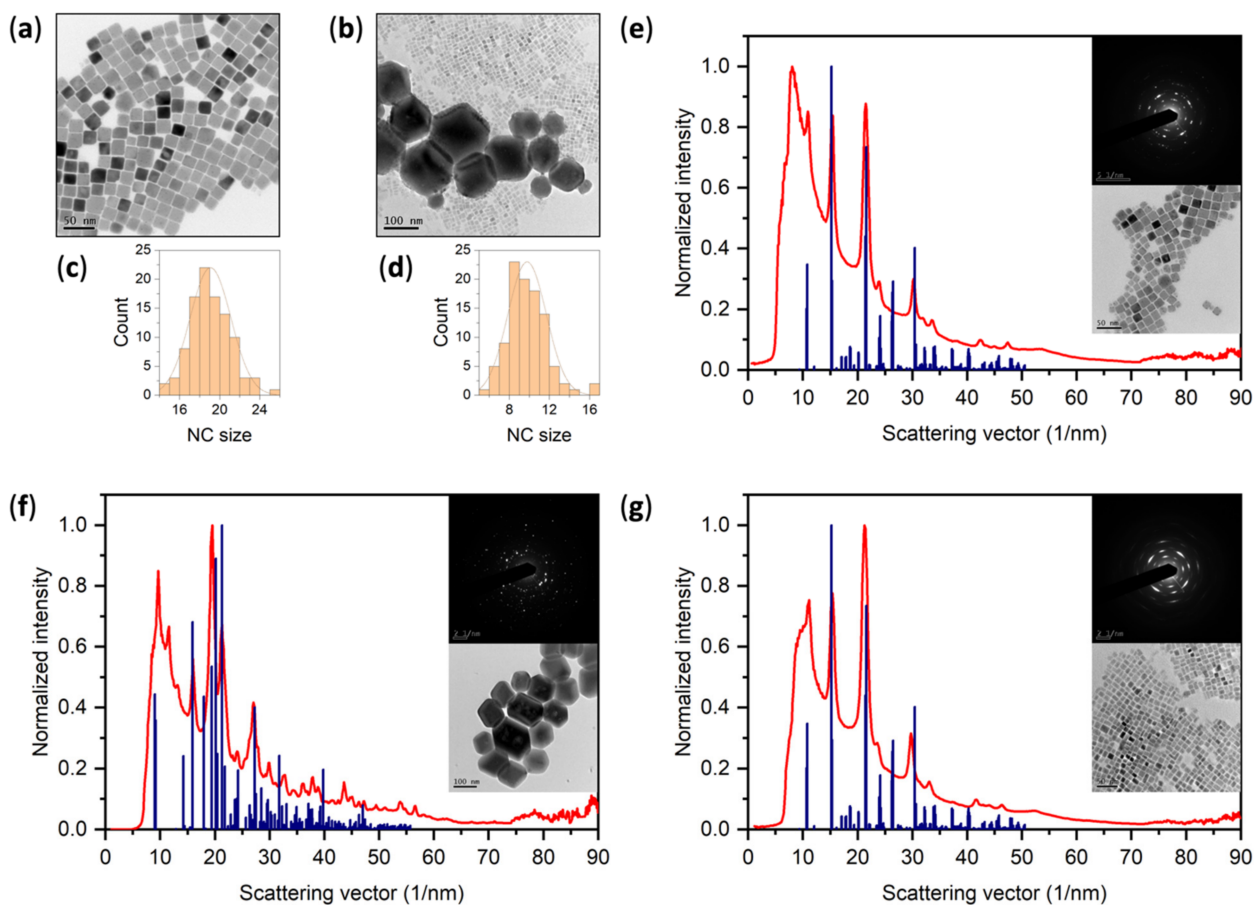


Figure 2. (a) TEM micrograph of the pure sample; (b) TEM micrograph of the mixed sample; (c) size distribution of 100 crystals presented in (a), the mean size is (19.1 ± 0.2) nm; (d) size distribution of 100 crystals presented in (b), the mean size is (9.8 ± 0.2) nm; (e) integrated radial intensity profile from a SAED pattern (in the inset) of the pure sample (corresponding micrograph in the inset) compared to the ICDD PDF-2 record for CsPbBr_3 #01-072-7929; (f) integrated radial intensity profile from a SAED pattern (in the inset) of large hexagonal crystals present in the mixed sample (corresponding micrograph in the inset) compared to the ICDD PDF-2 record for Cs_4PbBr_6 #01-077-8224; and (g) integrated radial intensity profile from a SAED pattern (in the inset) of small cubic crystals present in the mixed sample (corresponding micrograph in the inset) compared to the ICDD PDF-2 record for CsPbBr_3 #01-072-7929. Sizes of nanocrystals were measured using an ImageJ software [51] and SAED patterns were integrated using the ProcessDiffraction software [52].

The reason we cannot see the CsPbBr_3 phase on XRPD clearly (only partially in the supernatant sample) is that Cs_4PbBr_6 crystals are one order of magnitude larger than CsPbBr_3 nanocrystals. In this case, XRPD is not capable of distinguishing the CsPbBr_3 phase present in minority, especially when consisting of smaller particles. We estimate that the amount of CsPbBr_3 phase in this sample was less than 5%. Any reflections from CsPbBr_3 nanocrystals are in this case destined to be lost in the background. CsPbBr_3 reflections were observable only on the supernatant sample, as the majority of large Cs_4PbBr_6 crystals were separated by centrifugation. However, due to the preferential orientation, which resulted from the drop-casting process, this XRPD analysis was not conclusive enough. When in any doubt, it is crucial to exploit more sensitive methods, such as SAED, which was performed in this work, or for example using the synchrotron radiation for XRPD analysis, to avoid any misleading preliminary conclusions.

Based on the XRPD analysis, we denote the HI-prepared sample as “the pure sample” and the RTP-prepared sample as “the mixed sample”.

Absorption spectra of all samples are presented in Figure 3a. Spectrum of pure CsPbBr_3 sample (green line) features typical CsPbBr_3 absorption edge at 515 nm. Absorp-

tion band peaking at 261 nm can be attributed to an excess of surfactants (this peak tends to diminish with lower concentration of nanocrystals, see the Supplementary Information Figure S2 for detailed explanation and additional spectra).

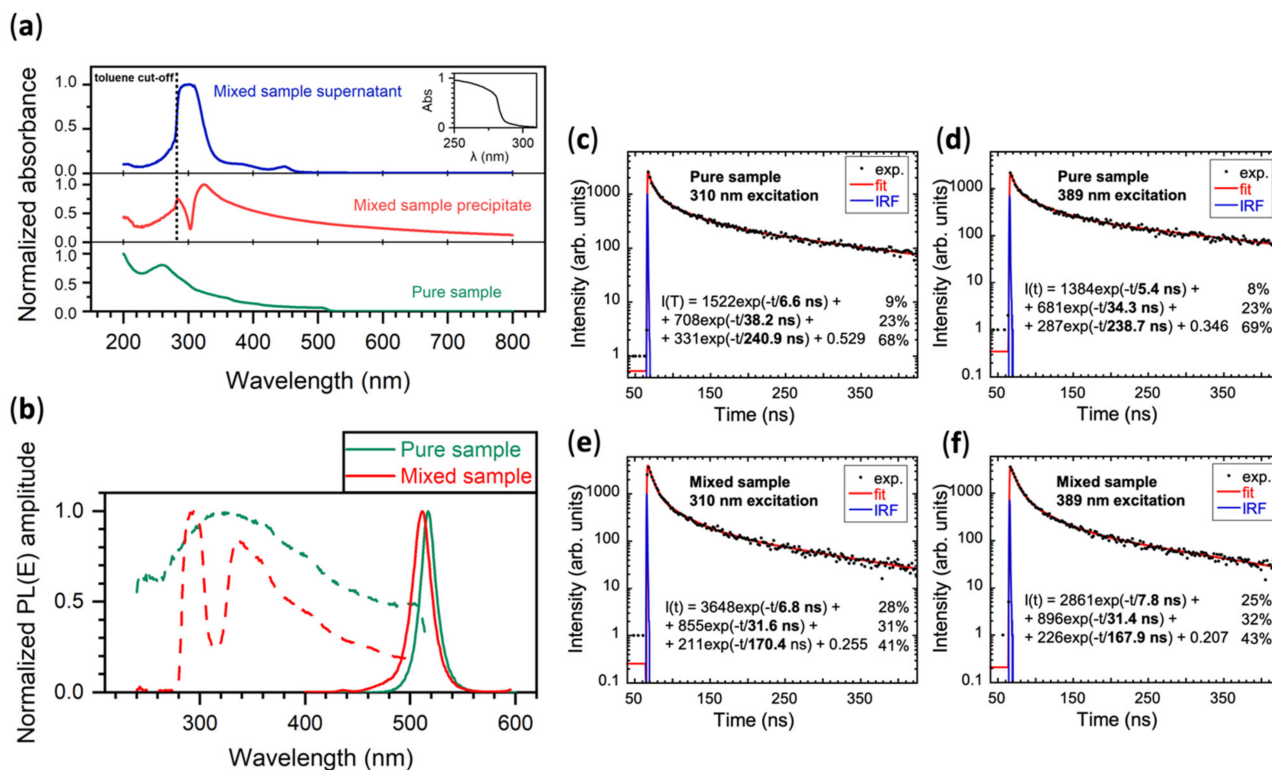


Figure 3. (a) Absorption spectra of both the supernatant (blue line) and precipitate (red line) of the mixed sample (in toluene) and that of the pure sample (green line, in hexane), in the inset: absorption spectrum of toluene; (b) PL characteristics of the pure sample (green lines) and the mixed sample (red lines), excitation spectra, collected at the emission maxima, are in dashed lines, emission spectra in solid lines, excitation wavelength was 300 nm in both cases; and (c–f) PL decay curves of both the pure (c,d) and mixed (e,f) samples, excited at 310 nm (c,e) and 389 nm (d,f). Black dots represent the experimental data, red line is the best fit (3-exponential function), and blue line is the instrumental response function (IRF).

Absorption spectrum of the mixed sample (red line) has a very high background caused by the light scattering at large Cs_4PbBr_6 crystals. We can identify broader absorption band peaking between 305–330 nm, which may be attributed to the bulk absorption of Cs_4PbBr_6 crystals [10,34,53]. Any possible CsPbBr_3 -related absorption edge is hidden in the background. The spectrum rapidly drops down below 283 nm; this is caused by the toluene cut-off (see the toluene absorption spectrum in the inset). The same artefact can be observed in the absorption spectrum of the supernatant of the mixed sample, but not in the spectrum of the pure sample, which is dispersed in hexane.

Absorption spectrum of the supernatant of the mixed sample is presented as a blue line in Figure 3a. This spectrum features two CsPbBr_3 -related absorption maxima at 449 nm and 385 nm, both significantly blue-shifted compared to the absorption of the pure sample. As discussed above (XRPD characterization), CsPbBr_3 nanocrystals present in this sample are probably in the form of nanoplatelets. Strong blue shift of absorption spectrum indicates that at least one dimension is below the exciton Bohr diameter ($\sim 4\text{--}7$ nm) [4,50], which further supports the nanoplatelets hypothesis. Based on this consideration, we may attribute the 385 nm and 449 nm absorption features to the light hole-electron and heavy hole-electron transitions, respectively. Another feature in this spectrum is an absorption at 310 nm, which can be attributed to absorption of Cs_4PbBr_6 crystals [34,54].

Figure 3b shows photoluminescence (PL) emission and excitation spectra of both samples. Spectra of the mixed sample's supernatant are presented in Supplementary

Information Figures S3–S5. Emission maximum of the mixed sample is blue shifted from the maximum of the pure sample by 6 nm, which is caused by the size difference of CsPbBr₃ nanocrystals. Excitation spectrum of the pure sample follows its absorption spectrum up to its maximum at 329 nm. However, excitation spectrum of the mixed sample features a significant drop in its intensity at 314 nm, which matches the Cs₄PbBr₆ absorption (similarly as in [55]).

Cs₄PbBr₆ has larger band gap than CsPbBr₃, therefore an energy transfer is theoretically possible. The drop in the mixed sample excitation spectra does not go all the way to zero intensity, so it does not rule out this possibility as well. We tested the following hypothesis (see Figure 4): Is it possible that the incident radiation excites the Cs₄PbBr₆ phase, and then the energy is either radiatively or non-radiatively transferred to the CsPbBr₃ phase? TEM shows that both phases are in a very close proximity, so both mechanisms are, in principle, possible, even if the radiative transfer has in this case generally much higher probability.

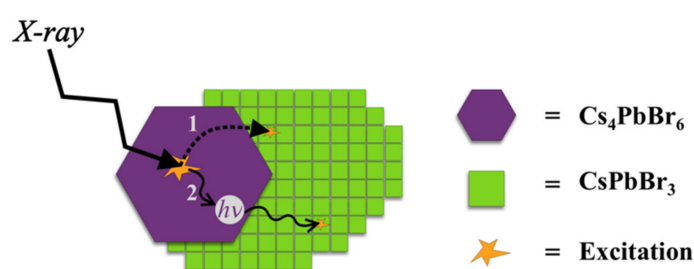


Figure 4. Schematic illustration of the energy-transfer hypothesis; **path 1:** non-radiative energy transfer from Cs₄PbBr₆ excited state to the excited state of neighboring CsPbBr₃ nanocrystal; **path 2:** radiative energy transfer, ultraviolet photon emitted by scintillation process in Cs₄PbBr₆ is absorbed by CsPbBr₃ nanocrystal.

In order to investigate the possible energy transfer between these two phases, we recorded PL decays at two excitation wavelengths for both the pure and the mixed sample. One wavelength (310 nm) was selected to excite mostly the Cs₄PbBr₆ phase, and the second (389 nm) to excite the CsPbBr₃ phase exclusively.

Decay curves of the pure sample are shown in Figure 3c,d. They are almost identical, featuring 6 ns fast decay component. Panels (e) and (f) show decay curves of the mixed sample. Again, they are almost identical, therefore no energy transfer from Cs₄PbBr₆ to CsPbBr₃ was confirmed. Moreover, compared to the pure sample, the fast components are roughly similar, only the slowest component seems to be faster in the mixed sample. Additionally, the contribution of the fastest component is significantly higher in the mixed sample.

This acceleration of the decay time in the mixed sample is probably caused by the presence of smaller CsPbBr₃ nanocrystals. One factor may be the quantum confinement effect, but it can also be caused by the luminescence quenching on various defects. It is well known that, in smaller nanocrystals with higher surface to volume ratio, more surface defects are present, which can be responsible for significant quenching. Nevertheless, the presence of Cs₄PbBr₆ phase seems to have no effect on PL temporal characteristics of the CsPbBr₃ nanocrystals, which might also be due to severe thermal quenching of the emission of the former at room temperature [34].

Due to the nature of the samples, it is challenging to guarantee the same concentration of the solid phase in both mixed and pure samples to reliably assess the quantitative effect of the Cs₄PbBr₆ presence on the CsPbBr₃ PL intensity. This is also the reason we present only normalized (to a maximum) PL spectra in Figure 3b. However, we can ensure the same thickness of the centrifuged solid samples for radioluminescence (RL) characterization, and thus provide the quantitative comparison in this set of data (cf. Figure 5). Moreover, as the

target application of our investigation is the high energy radiation detection, quantitative changes in scintillation (unlike PL) parameters are those of real interest.

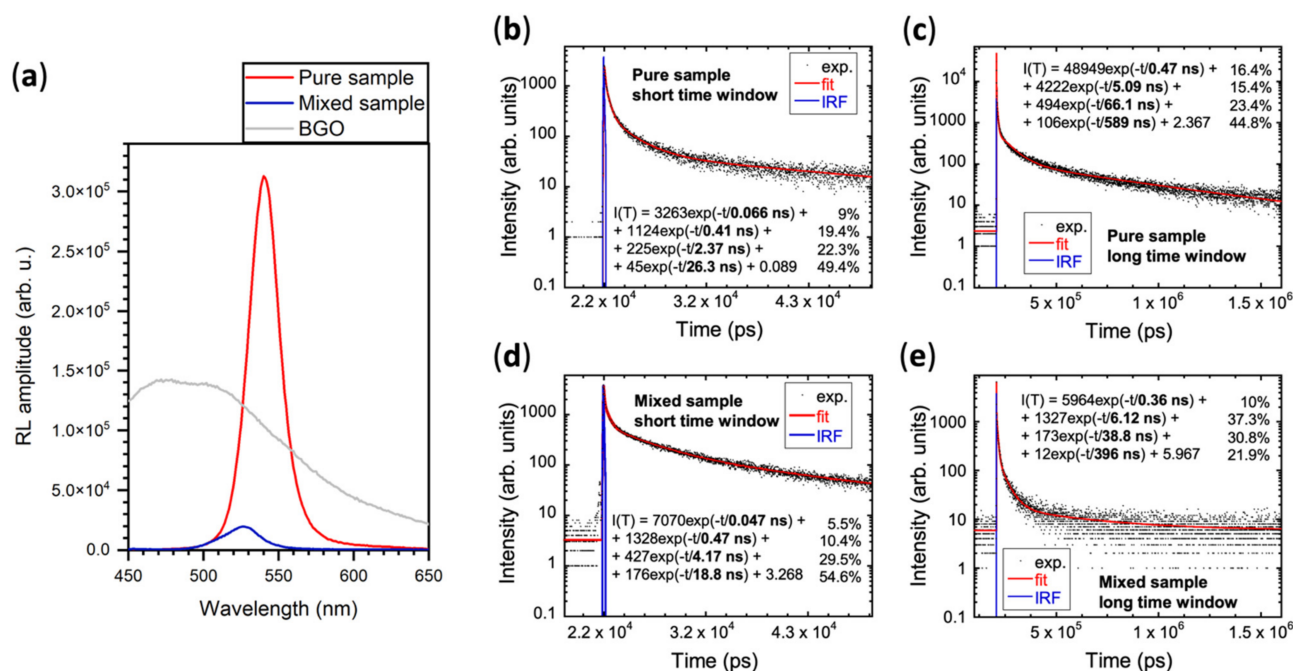


Figure 5. (a) Radioluminescence (RL) spectra of the pure sample (red line) and of the mixed sample (blue line) compared to the RL spectrum of Bi₄Ge₃O₁₂ (BGO) powder (grey line); (b–e) scintillation decay curves for both the pure (b,c) and mixed (d,e) samples, recorded in both the short (b,d) and long (c,e) time windows. Black dots represent the experimental data, red line is the best fit (4-exponential function), and blue line is the instrumental response function (IRF).

Figure 5 summarizes RL characterization of both samples with powder Bi₃Ge₄O₁₂ (BGO) standard scintillator used for a comparison. Steady state RL spectrum in panel (a) shows that intensity of the pure sample is one order of magnitude larger than that of the mixed sample. One factor contributing to such difference may be the abovementioned higher concentration of surface defects resulting from the smaller CsPbBr₃ nanocrystals present in the mixed sample. However, this alone would not cause such a strong effect. Furthermore, it can be expected that CsPbBr₃ nanocrystals prepared at room temperature by rapid precipitation process would have poorer crystallinity, more crystallographic defects, and, subsequently, lower PLQY, compared to nanocrystals precipitated at elevated temperatures during the hot injection process. However, we have never encountered any evidence in the literature about CsPbBr₃ nanocrystals prepared by the precipitation method and compared to CsPbBr₃ nanocrystals prepared by the hot injection in the same lab to have such poor photoluminescence properties that could result in one order of magnitude difference in scintillation light output.

On the other hand, the presence of Cs₄PbBr₆ crystals in the sample is capable of significantly deteriorating the bright luminescence of CsPbBr₃ nanocrystals due to the emission dumping effect at Cs₄PbBr₆ caused by its strong quenching [34]. Figure 3b shows a significant drop in the excitation spectrum of CsPbBr₃ emission resulting from the Cs₄PbBr₆ absorption. Neither PL decay measurements in Figure 3, nor scintillation decay measurements in Figure 5, indicate any form of energy transfer from Cs₄PbBr₆ to the CsPbBr₃ phase (due to thermal quenching of its emission). Therefore, all the energy that is deposited in Cs₄PbBr₆ crystals is lost to the scintillation process in CsPbBr₃. Moreover, Cs₄PbBr₆ crystals are one order of magnitude larger than CsPbBr₃ nanocrystals in the mixed sample, therefore they are more capable of efficient stopping the incident X-ray radiation. In addition, they are diluting the CsPbBr₃ concentration in this sample, which

further reduces the probability of effective deposition of incident radiation energy in the CsPbBr₃ phase.

Furthermore, incident radiation generates excitons, or self-trapped electrons and holes, in the Cs₄PbBr₆ lattice. When localized charge carriers diffusing through Cs₄PbBr₆ encounter large and fairly even offset at the conduction and valence band edges (Cs₄PbBr₆ vs. CsPbBr₃), they will likely dissociate, and it may serve to concentrate carriers in CsPbBr₃ [46]. Smaller Cs₄PbBr₆ particles would trigger shorter diffusion length and consequently higher probability of dissociation and charge transfer to CsPbBr₃, again resulting in better efficiency and yield of green emission.

The larger the Cs₄PbBr₆ crystals, the more prominent the above-described effects reducing the overall RL intensity.

Therefore, we conclude that the presence of Cs₄PbBr₆ crystals alongside CsPbBr₃ nanocrystals significantly reduces their scintillation light output.

This conclusion supports theoretical prediction published in the recent Perspective [45]. They considered a CsPbBr₃@Cs₄PbBr₆ quantum-dot-in-host-like composite, and calculated a PL spectrum escaping from 10 μm depth within the sample. They found that, compared to the launched PL spectrum, the escaping one is 100× attenuated and red-shifted by 20 nm. Our experiments qualitatively confirm this weakening of CsPbBr₃ light output in the presence of Cs₄PbBr₆ phase. Our systems were not identical, but in both cases, it was the CsPbBr₃ nanocrystalline phase surrounded by a larger amount of Cs₄PbBr₆ phase in some form, therefore we believe that this comparison is justified. We also confirm a significant red shift (15 nm) between the PL spectrum of colloidal sample (i.e., “launched” spectrum) and RL spectrum of precipitated powder (i.e., “escaping” spectrum from within the sample). This red shift also occurs in the pure sample, where it is even larger (23 nm) due to the higher concentration of absorbing CsPbBr₃ nanocrystals (Cs₄PbBr₆ phase does not absorb the 517 nm light).

Scintillation decay curves of both samples are similar within the uncertainty given by the 4-exponential approximation. They all feature two sub-nanosecond components (50 ps and 400 ps), which is a crucial property for the intended fast timing applications.

The presence of Cs₄PbBr₆ phase does not affect luminescence properties of the sample, other than the scintillation light output. Therefore, for most optoelectronic applications, its presence does not hinder successful implementation. It can even prove beneficial in protecting CsPbBr₃ nanocrystals from a deteriorative effect of air oxygen and humidity, as in [23–25]. However, for applications such as scintillation detectors for fast timing, the drop in the CsPbBr₃ radioluminescence intensity can become detrimental.

4. Conclusions

We synthesized and characterized CsPbBr₃ nanocrystals prepared by the hot injection method (HI) and their mixture with Cs₄PbBr₆ crystals using the room temperature precipitation method (RTP), which we compared and evaluated with respect to possible future optoelectronic applications. Our RTP protocol yields high amount of Cs₄PbBr₆ phase, which allowed us to study its possible effect on the CsPbBr₃ luminescence properties.

We demonstrated that the Cs₄PbBr₆ crystals have significant negative impact on the CsPbBr₃ scintillation light output, most probably due to strong thermal quenching of their luminescence, but do not affect timing properties in any way. This conclusion supports theoretical predictions in [45] even if our system was not identical. We believe that this is another step towards better understanding of such materials regarding their scintillation characteristics. Moreover, our study did not provide any sufficient evidence of an energy transfer between those two phases.

We conclude that the presence of Cs₄PbBr₆ phase should be a concern for any optoelectronic application requiring high scintillation light output, such as scintillation detectors for fast timing applications. In this case, much attention needs to be paid to characterization of the material prepared by the RTP process to rule out the possible presence of Cs₄PbBr₆

phase, especially when thinking of upscaling for large batches for possible future industrial production.

Supplementary Materials: The following are available online at <https://www.mdpi.com/article/10.3390/nano11081935/s1>, Figure S1: Structure of CsPbBr₃ and Cs₄PbBr₆ drawn with VESTA software [S1], details on syntheses, Figure S2: Absorption spectra of the pure sample dispersed in hexane in three different concentrations; absorption spectra of the surfactants in the inset, Figure S3: Emission spectrum (excited at 300 nm) of the mixed sample and corresponding excitation spectra for each emission band, Figure S4: Gaussian decomposition of the mixed sample emission spectrum, and Figure S5: Comparison of PL of both samples excited by the 365 nm UV light. Reference [56] is cited in the supplementary materials.

Author Contributions: Conceptualization, M.N. and V.Č.; Formal analysis, K.D., A.S., J.K., I.J., V.J. and V.B.; Funding acquisition, E.M. and V.Č.; Investigation, K.D., A.S., J.K., I.J., V.J. and V.B.; Supervision, M.N., E.M. and V.Č.; Visualization, K.D.; Writing—original draft, K.D.; Writing—review and editing, K.D., A.S., J.K., M.N., V.J., V.B., E.M. and V.Č. All authors have read and agreed to the published version of the manuscript.

Funding: This research was funded by the Czech Science Foundation, grant number GA20-06374S, the Ministry of Education Youth and Sports, project “Center for advanced applied science”, grant number CZ.02.1.01/0.0/0.0/16_019/0000778 and by the Grant Agency of the Czech Technical University in Prague, grant number SGS20/185/OHK4/3T/14.

Institutional Review Board Statement: Not applicable.

Informed Consent Statement: Not applicable.

Data Availability Statement: The data presented in this study are available on request from the corresponding author.

Acknowledgments: This work was carried out in the frame of Crystal Clear Collaboration. The authors at CTU would like to express thanks to Benoit Mahler from UCB Lyon 1 for his invaluable advice regarding the hot injection methods.

Conflicts of Interest: The authors declare no conflict of interest.

References

1. Nikl, M.; Nitsch, K.; Polák, K.; Pazzi, G.P.; Fabeni, P.; Citrin, D.S.; Gurioli, M. Optical properties of the Pb²⁺-based aggregated phase in a CsCl host crystal: Quantum-confinement effects. *Phys. Rev. B* **1995**, *51*, 5192–5199. [[CrossRef](#)]
2. Babin, V.; Fabeni, P.; Nikl, M.; Nitsch, K.; Pazzi, G.P.; Zazubovich, S. Luminescent CsPbI₃ and Cs₄PbI₆ aggregates in annealed CsI:Pb crystals. *Phys. Status Solidi* **2001**, *226*, 419–428. [[CrossRef](#)]
3. Nikl, M.; Nitsch, K.; Míhóková, E.; Polák, K.; Fabeni, P.; Pazzi, G.P.; Gurioli, M.; Santucci, S.; Phani, R.; Scacco, A.; et al. Luminescence of CsPbBr₃-like quantum dots in CsBr single crystals. *Phys. E Low Dimens. Syst. Nanostruct.* **1999**, *4*, 323–331. [[CrossRef](#)]
4. Protesescu, L.; Yakunin, S.; Bodnarchuk, M.I.; Krieg, F.; Caputo, R.; Hendon, C.H.; Yang, R.X.; Walsh, A.; Kovalenko, M.V. Nanocrystals of cesium lead halide perovskites (CsPbX₃, X = Cl, Br, and I): Novel optoelectronic materials showing bright emission with wide color gamut. *Nano Lett.* **2015**, *15*, 3692–3696. [[CrossRef](#)] [[PubMed](#)]
5. Kulbak, M.; Gupta, S.; Kedem, N.; Levine, I.; Bendikov, T.; Hodes, G.; Cahen, D. Cesium enhances long-term stability of lead bromide perovskite-based solar cells. *J. Phys. Chem. Lett.* **2016**, *7*, 167–172. [[CrossRef](#)]
6. Song, Y.H.; Yoo, J.S.; Kang, B.K.; Choi, S.H.; Ji, E.K.; Jung, H.S.; Yoon, D.H. Long-term stable stacked CsPbBr₃ quantum dot films for highly efficient white light generation in LEDs. *Nanoscale* **2016**, *8*, 19523–19526. [[CrossRef](#)]
7. Swarnkar, A.; Chulliyil, R.; Ravi, V.K.; Irfanullah, M.; Chowdhury, A.; Nag, A. Colloidal CsPbBr₃ perovskite nanocrystals: Luminescence beyond traditional quantum dots. *Angew. Chem. Int. Ed.* **2015**, *54*, 15424–15428. [[CrossRef](#)]
8. Gandini, M.; Villa, I.; Beretta, M.; Gotti, C.; Imran, M.; Carulli, F.; Fantuzzi, E.; Sassi, M.; Zaffalon, M.; Brofferio, C.; et al. Efficient, fast and reabsorption-free perovskite nanocrystal-based sensitized plastic scintillators. *Nat. Nanotechnol.* **2020**, *15*, 462–468. [[CrossRef](#)]
9. Zhang, Y.; Sun, R.; Ou, X.; Fu, K.; Chen, Q.; Ding, Y.; Xu, L.-J.; Liu, L.; Han, Y.; Malko, A.V.; et al. Metal halide perovskite nanosheet for X-ray high-resolution scintillation imaging screens. *ACS Nano* **2019**, *13*, 2520–2525. [[CrossRef](#)]
10. Chen, Q.; Wu, J.; Ou, X.; Huang, B.; Almutlaq, J.; Zhumekenov, A.A.; Guan, X.; Han, S.; Liang, L.; Yi, Z.; et al. All-inorganic perovskite nanocrystal scintillators. *Nature* **2018**, *561*, 88–93. [[CrossRef](#)]

11. Mykhaylyk, V.B.; Kraus, H.; Kapustianyk, V.; Kim, H.J.; Mercere, P.; Rudko, M.; Da Silva, P.; Antonyak, O.; Dendebera, M. Bright and fast scintillations of an inorganic halide perovskite CsPbBr₃ crystal at cryogenic temperatures. *Sci. Rep.* **2020**, *10*, 1–11. [[CrossRef](#)]
12. Li, Y.; Shao, W.; Chen, L.; Wang, J.; Nie, J.; Zhang, H.; Zhang, S.; Gao, R.; Ouyang, X.; Ouyang, X.; et al. Lead-halide Cs₄PbBr₆ single crystals for high-sensitivity radiation detection. *NPG Asia Mater.* **2021**, *13*, 40. [[CrossRef](#)]
13. Moseley, O.D.I.; Doherty, T.A.S.; Parmee, R.; Anaya, M.; Stranks, S.D. Halide perovskites scintillators: Unique promise and current limitations. *J. Mater. Chem. C* **2021**. [[CrossRef](#)]
14. Yang, H.; Li, H.; Yuan, R.; Chen, J.; Zhao, J.; Wang, S.; Liu, Y.; Li, Q.; Zhang, Z. A novel scintillation screen for achieving high-energy ray detection with fast and full-color emission. *J. Mater. Chem. C* **2021**, 7905–7909. [[CrossRef](#)]
15. Luo, B.; Naghadeh, S.B.; Zhang, J.Z. Lead halide perovskite nanocrystals: Stability, surface passivation, and structural control. *ChemNanoMat* **2017**, *3*, 456–465. [[CrossRef](#)]
16. Leijtens, T.; Hoke, E.T.; Grancini, G.; Slotcavage, D.J.; Eperon, G.E.; Ball, J.M.; De Bastiani, M.; Bowering, A.R.; Martino, N.; Wojciechowski, K.; et al. Mapping electric field-induced switchable poling and structural degradation in hybrid lead halide perovskite thin films. *Adv. Energy Mater.* **2015**, *5*, 1–11. [[CrossRef](#)]
17. Guan, H.; Zhao, S.; Wang, H.; Yan, D.; Wang, M.; Zang, Z. Room temperature synthesis of stable single silica-coated CsPbBr₃ quantum dots combining tunable red emission of Ag–In–Zn–S for High-CRI white light-emitting diodes. *Nano Energy* **2020**, *67*, 104279. [[CrossRef](#)]
18. Shao, H.; Bai, X.; Pan, G.; Cui, H.; Zhu, J.; Zhai, Y.; Liu, J.; Dong, B.; Xu, L.; Song, H. Highly efficient and stable blue-emitting CsPbBr₃@SiO₂ nanospheres through low temperature synthesis for nanoprinting and WLED. *Nanotechnology* **2018**, *29*, 285706. [[CrossRef](#)]
19. Zhong, Q.; Cao, M.; Hu, H.; Yang, D.; Chen, M.; Li, P.; Wu, L.; Zhang, Q. One-pot synthesis of highly stable CsPbBr₃@SiO₂ core-shell nanoparticles. *ACS Nano* **2018**, *12*, 8579–8587. [[CrossRef](#)] [[PubMed](#)]
20. Li, Z.J.; Hofman, E.; Li, J.; Davis, A.H.; Tung, C.H.; Wu, L.Z.; Zheng, W. Photoelectrochemically active and environmentally stable CsPbBr₃/TiO₂ core/shell nanocrystals. *Adv. Funct. Mater.* **2018**, *28*, 1–7. [[CrossRef](#)]
21. Yang, W.; Gao, F.; Qiu, Y.; Liu, W.; Xu, H.; Yang, L.; Liu, Y. CsPbBr₃-quantum-dots/Polystyrene@Silica hybrid microsphere structures with significantly improved stability for white LEDs. *Adv. Opt. Mater.* **2019**, *7*, 1–12. [[CrossRef](#)]
22. Cai, Y.; Wang, L.; Zhou, T.; Zheng, P.; Li, Y.; Xie, R.J. Improved stability of CsPbBr₃ perovskite quantum dots achieved by suppressing interligand proton transfer and applying a polystyrene coating. *Nanoscale* **2018**, *10*, 21441–21450. [[CrossRef](#)]
23. He, M.; Wang, C.; Li, J.; Wu, J.; Zhang, S.; Kuo, H.C.; Shao, L.; Zhao, S.; Zhang, J.; Kang, F.; et al. CsPbBr₃-Cs₄PbBr₆ composite nanocrystals for highly efficient pure green light emission. *Nanoscale* **2019**, *11*, 22899–22906. [[CrossRef](#)]
24. Chen, Y.M.; Zhou, Y.; Zhao, Q.; Zhang, J.Y.; Ma, J.P.; Xuan, T.T.; Guo, S.Q.; Yong, Z.J.; Wang, J.; Kuroiwa, Y.; et al. Cs₄PbBr₆/CsPbBr₃ Perovskite composites with near-unity luminescence quantum yield: Large-scale synthesis, luminescence and formation mechanism, and white light-emitting diode application. *ACS Appl. Mater. Interfaces* **2018**, *10*, 15905–15912. [[CrossRef](#)] [[PubMed](#)]
25. Xu, J.; Huang, W.; Li, P.; Onken, D.R.; Dun, C.; Guo, Y.; Ucer, K.B.; Lu, C.; Wang, H.; Geyer, S.M.; et al. Imbedded nanocrystals of CsPbBr₃ in Cs₄PbBr₆: Kinetics, enhanced oscillator strength, and application in light-emitting diodes. *Adv. Mater.* **2017**, *29*, 1–10. [[CrossRef](#)]
26. Grandhi, G.K.; Viswanath, N.S.M.; Cho, H.B.; Kim, S.M.; Im, W. Bin Highly stable hetero-structured green-emitting cesium lead bromide nanocrystals: Via ligand-mediated phase control. *Nanoscale* **2019**, *11*, 21137–21146. [[CrossRef](#)]
27. Jing, Q.; Xu, Y.; Su, Y.; Xing, X.; Lu, Z. A systematic study of the synthesis of cesium lead halide nanocrystals: Does Cs₄PbBr₆ or CsPbBr₃ form? *Nanoscale* **2019**, *11*, 1784–1789. [[CrossRef](#)]
28. Cao, F.; Yu, D.; Xu, X.; Han, Z.; Zeng, H. CsPbBr₃@Cs₄PbBr₆ Emitter-in-host composite: Fluorescence origin and interphase energy transfer. *J. Phys. Chem. C* **2021**, *125*, 3–19. [[CrossRef](#)]
29. Saidaminov, M.I.; Almutlaq, J.; Sarmah, S.; Dursun, I.; Zhumekenov, A.A.; Begum, R.; Pan, J.; Cho, N.; Mohammed, O.F.; Bakr, O.M. Pure Cs₄PbBr₆: Highly luminescent zero-dimensional perovskite solids. *ACS Energy Lett.* **2016**, *1*, 840–845. [[CrossRef](#)]
30. Zhang, Y.; Saidaminov, M.I.; Dursun, I.; Yang, H.; Murali, B.; Alarousu, E.; Yengel, E.; Alshankiti, B.A.; Bakr, O.M.; Mohammed, O.F. Zero-dimensional Cs₄PbBr₆ perovskite nanocrystals. *J. Phys. Chem. Lett.* **2017**, *8*, 961–965. [[CrossRef](#)]
31. Qin, Z.; Dai, S.; Hadjiev, V.G.; Wang, C.; Xie, L.; Ni, Y.; Wu, C.; Yang, G.; Chen, S.; Deng, L.; et al. Revealing the origin of luminescence center in 0D Cs₄PbBr₆ perovskite. *Chem. Mater.* **2019**, *31*, 9098–9104. [[CrossRef](#)]
32. Xu, Q.; Wang, J.; Shao, W.; Ouyang, X.; Wang, X.; Zhang, X.; Guo, Y.; Ouyang, X. A solution-processed zero-dimensional all-inorganic perovskite scintillator for high resolution gamma-ray spectroscopy detection. *Nanoscale* **2020**, *12*, 9727–9732. [[CrossRef](#)]
33. Kostopoulou, A.; Brintakis, K.; Serpetzoglou, E.; Stratakis, E. Laser-assisted fabrication for metal halide perovskite-2D nanoconjugates: Control on the nanocrystal density and morphology. *Nanomaterials* **2020**, *10*, 747. [[CrossRef](#)] [[PubMed](#)]
34. Nikl, M.; Mihóková, E.; Nitsch, K.; Somma, F.; Giampaolo, C.; Pazzi, G.; Fabeni, P.; Zazubovich, S. Photoluminescence of Cs₄PbBr₆ crystals and thin films. *Chem. Phys. Lett.* **1999**, *306*, 280–284. [[CrossRef](#)]
35. Yang, L.; Li, D.; Wang, C.; Yao, W.; Wang, H.; Huang, K. Room-temperature synthesis of pure perovskite-related Cs₄PbBr₆ nanocrystals and their ligand-mediated evolution into highly luminescent CsPbBr₃ nanosheets. *J. Nanopart. Res.* **2017**, *19*, 258. [[CrossRef](#)]

36. Rao, L.; Ding, X.; Du, X.; Liang, G.; Tang, Y.; Tang, K.; Zhang, J.Z. Ultrasonication-assisted synthesis of CsPbBr₃ and Cs₄PbBr₆ perovskite nanocrystals and their reversible transformation. *Beilstein J. Nanotechnol.* **2019**, *10*, 666–676. [[CrossRef](#)]
37. Palazon, F.; Urso, C.; De Trizio, L.; Akkerman, Q.; Marras, S.; Locardi, F.; Nelli, I.; Ferretti, M.; Prato, M.; Manna, L. Postsynthesis transformation of insulating Cs₄PbBr₆ nanocrystals into bright perovskite CsPbBr₃ through physical and chemical extraction of CsBr. *ACS Energy Lett.* **2017**, *2*, 2445–2448. [[CrossRef](#)]
38. Baranov, D.; Caputo, G.; Goldoni, L.; Dang, Z.; Scarfiello, R.; De Trizio, L.; Portone, A.; Fabbri, F.; Camposeo, A.; Pisignano, D.; et al. Transforming colloidal Cs₄PbBr₆ nanocrystals with poly(maleic anhydride-alt -1-octadecene) into stable CsPbBr₃ perovskite emitters through intermediate heterostructures. *Chem. Sci.* **2020**, *11*, 3986–3995. [[CrossRef](#)]
39. Akkerman, Q.A.; Park, S.; Radicchi, E.; Nunzi, F.; Mosconi, E.; De Angelis, F.; Brescia, R.; Rastogi, P.; Prato, M.; Manna, L. Nearly monodisperse insulator Cs₄PbX₆ (X = Cl, Br, I) nanocrystals, their mixed halide compositions, and their transformation into CsPbX₃ nanocrystals. *Nano Lett.* **2017**, *17*, 1924–1930. [[CrossRef](#)]
40. Yin, J.; Yang, H.; Song, K.; El-Zohry, A.M.; Han, Y.; Bakr, O.M.; Brédas, J.L.; Mohammed, O.F. Point defects and green emission in zero-dimensional perovskites. *J. Phys. Chem. Lett.* **2018**, *9*, 5490–5495. [[CrossRef](#)]
41. Cha, J.H.; Lee, H.J.; Kim, S.H.; Ko, K.C.; Suh, B.J.; Han, O.H.; Jung, D.Y. Superparamagnetism of green emissive Cs₄PbBr₆ zero-dimensional perovskite crystals. *ACS Energy Lett.* **2020**, *5*, 2208–2216. [[CrossRef](#)]
42. Yang, L.; Wang, T.; Yang, X.; Zhang, M.; Pi, C.; Yu, J.; Zhou, D.; Yu, X.; Qiu, J.; Xu, X. Extrinsic photoluminescence properties of individual micro-particle of Cs₄PbBr₆ perovskite with “defect” structure. *Opt. Express* **2019**, *27*, 31207. [[CrossRef](#)]
43. Lecoq, P.; Morel, C.; Prior, J.O.; Visvikis, D.; Gundacker, S.; Auffray, E.; Križan, P.; Turtos, R.M.; Thers, D.; Charbon, E.; et al. Roadmap toward the 10 ps time-of-flight PET challenge. *Phys. Med. Biol.* **2020**, *65*, 21RM01. [[CrossRef](#)]
44. Tomanová, K.; Suchá, A.; Mihóková, E.; Procházková, L.; Jakubec, I.; Turtos, R.M.; Gundacker, S.; Auffray, E.; Čuba, V. CsPbBr₃ thin films on LYSO:Ce substrates. *IEEE Trans. Nucl. Sci.* **2020**, *67*, 933–938. [[CrossRef](#)]
45. Williams, R.T.; Wolszczak, W.W.; Yan, X.; Carroll, D.L. Perovskite quantum-dot-in-host for detection of ionizing radiation. *ACS Nano* **2020**, *14*, 5161–5169. [[CrossRef](#)] [[PubMed](#)]
46. Kang, B.; Biswas, K. Exploring polaronic, excitonic structures and luminescence in Cs₄PbBr₆/CsPbBr₃. *J. Phys. Chem. Lett.* **2018**, *9*, 830–836. [[CrossRef](#)]
47. Cao, F.; Yu, D.; Ma, W.; Xu, X.; Cai, B.; Yang, Y.M.; Liu, S.; He, L.; Ke, Y.; Lan, S.; et al. shining emitter in a stable host: Design of halide perovskite scintillators for X-ray imaging from commercial concept. *ACS Nano* **2020**, *14*, 5183–5193. [[CrossRef](#)]
48. Li, X.; Wu, Y.; Zhang, S.; Cai, B.; Gu, Y.; Song, J.; Zeng, H. CsPbX₃ quantum dots for lighting and displays: Room-temperature synthesis, photoluminescence superiorities, underlying origins and white light-emitting diodes. *Adv. Funct. Mater.* **2016**, *26*, 2435–2445. [[CrossRef](#)]
49. Lu, C.; Wright, M.W.; Ma, X.; Li, H.; Itanze, D.S.; Carter, J.A.; Hewitt, C.A.; Donati, G.L.; Carroll, D.L.; Lundin, P.M.; et al. Cesium oleate precursor preparation for lead halide perovskite nanocrystal synthesis: The influence of excess oleic acid on achieving solubility, conversion, and reproducibility. *Chem. Mater.* **2019**, *31*, 62–67. [[CrossRef](#)]
50. Tomanová, K.; Čuba, V.; Brik, M.G.; Mihóková, E.; Martínez Turtos, R.; Lecoq, P.; Auffray, E.; Nikl, M. On the structure, synthesis, and characterization of ultrafast blue-emitting CsPbBr₃ nanoplatelets. *APL Mater.* **2019**, *7*, 011104. [[CrossRef](#)]
51. Abràmoff, M.D.; Magalhães, P.J.; Ram, S.J. Image processing with imageJ. *Biophotonics Int.* **2004**, *11*, 36–41. [[CrossRef](#)]
52. Lábár, J.L. “ProcessDiffraction”: A computer program to process electron diffraction patterns from polycrystalline or amorphous samples. *Proc. Eurem* **2000**, *3*, I379–I380.
53. Zhang, Z.; Zhu, Y.; Wang, W.; Zheng, W.; Lin, R.; Li, X.; Zhang, H.; Zhong, D.; Huang, F. Aqueous solution growth of millimeter-sized nongreen-luminescent wide bandgap Cs₄PbBr₆ bulk crystal. *Cryst. Growth Des.* **2018**, *18*, 6393–6398. [[CrossRef](#)]
54. Kondo, S.; Amaya, K.; Saito, T. Localized optical absorption in Cs₄PbBr₆. *J. Phys. Condens. Matter* **2002**, *14*, 2093–2099. [[CrossRef](#)]
55. Quan, L.N.; Quintero-Bermudez, R.; Voznyy, O.; Walters, G.; Jain, A.; Fan, J.Z.; Zheng, X.; Yang, Z.; Sargent, E.H. Highly emissive green perovskite nanocrystals in a solid state crystalline matrix. *Adv. Mater.* **2017**, *29*, 1–6. [[CrossRef](#)]
56. Momma, K.; Izumi, F. VESTA3 for three-dimensional visualization of crystal, volumetric and morphology data. *J. Appl. Crystallogr.* **2011**, *44*, 1272–1276. [[CrossRef](#)]